Laser and Particle Beams

cambridge.org/lpb

A high-energy electron density modulator driven by an intense laser standing wave

Shiyi Zhou[1,2,*], Zhijun Zhang[1,*], Chuliang Zhou[1], Zhongpeng Li[1], Ye Tian[1,2] and Jiansheng Liu[1,3–5]

[1]State Key Laboratory of High Field Laser Physics, Shanghai Institute of Optics and Fine Mechanics, Chinese Academy of Sciences, Shanghai 201800, China; [2]Center of Materials Science and Optoelectronics Engineering, University of Chinese Academy of Sciences, Beijing 100049, China; [3]Department of Physics, Shanghai Normal University, Shanghai 200234, China; [4]IFSA Collaborative Innovation Center, Shanghai Jiao Tong University, Shanghai 200240, China and [5]Institute of Modern Optics, Nankai University, Tianjing 300000, China

Research Article

*Shiyi Zhou and Zhijun Zhang contributed equally to this paper.

Cite this article: Zhou S, Zhang Z, Zhou C, Li Z, Tian Y, Liu J (2019). A high-energy electron density modulator driven by an intense laser standing wave. *Laser and Particle Beams* **37**, 197–202. https://doi.org/10.1017/S0263034619000338

Received: 9 January 2019
Revised: 13 March 2019
Accepted: 22 March 2019

Key words:
Laser standing wave field; relativistic electron beam; ponderomotive force

Author for correspondence:
Ye Tian, State Key Laboratory of High Field Laser Physics. Jiansheng Liu, Shanghai Institute of Optics and Fine Mechanics, Chinese Academy of Sciences, Shanghai 201800, China. E-mails: tianye@siom.ac.cn, michaeljs_liu@siom.ac.cn

Abstract

A high energy electron density modulator from a high-intensity laser standing wave field is studied herein by investigating the ultrafast motion of electrons in the field. Electrons converge at the electric field antinodes, and the discrete electron density peaks modulated by the field located at the corresponding laser phases of $kx = n\pi$, ($n = 0, 1, 2, \ldots$), that is, the modulation period is 1/2 the wavelength of the individual laser. We also discussed the influence of the laser parameters such as laser intensity and waist size on the beam modulator. It is shown that a long interaction length (waist) or sufficiently high field intensity is essential for relativistic electron density modulation.

Introduction

The intense laser control of high-energy particles has made significant progress in the past decade, and is highly promising for high-energy electron generation, ion acceleration (Tajima and Dawson, 1979; Faure *et al.*, 2004; Geddes *et al.*, 2004; Mangles *et al.*, 2004; Calendron *et al.*, 2018), and electron microscopy (Zewail, 2006, 2010; Sciaini and Miller, 2011; Flannigan and Zewail, 2012). The considerable progress in superpower laser sources and plasma-accelerator technologies (Schaeffer *et al.*, 2018) has enabled the energy of electrons of more than multi-GeV in centimeters. Meanwhile, ultrafast MeV electron sources have enabled the time-resolved imaging of fundamental processes in diverse fields such as solid state physics (Bloch *et al.*, 2008), chemistry (Juffmann *et al.*, 2012), and biology (Germann *et al.*, 2010). However, from the perspective of controlling high-energy electrons by lasers, laser standing waves have been used to construct matter interferometers for atoms (Gould *et al.*, 1986). The advantage of using laser standing waves for controlling electrons is that the materials need not be near the electrons, thus allowing for electron sources in the high-energy range.

A significant all-optical electron beam manipulation is a standing electromagnetic wave scattering of electrons, and is described as Kapitza–Dirac effects first proposed in 1933 (Kapitza and Dirac, 1933). This electron scattering is the quintessential expression of the wave–particle duality with massive particles, in which the electrons are treated as waves when transported through standing-wave light. In the following years, widely theoretical (Bartell, 1967; Fedorov, 1967) and experimental (Bucksbaum *et al.*, 1987, 1988; Moore *et al.*, 1995; Freimund *et al.*, 2001) investigations about this effect have been developed. Early convincing experimental demonstrations shown by Bucksbaum *et al.* provided the result of low-energy photoelectrons scattered in an intense optical standing wave referred to as multiphoton ionization (Hollis, 1978; Fiordilino and Mittleman, 1985; Freeman *et al.*, 1986). The diffraction of free electrons from a standing light wave described as coherent interference differs from the previous observation where rainbow scattering peaks was not coherent (Freimund *et al.*, 2001). Theoretically, this process was interpreted with quantum mechanics treatments (Li *et al.*, 2004; Batelaan, 2007) as well as classical treatments (Chan and Tsui, 1979; Efremov and Fedorov, 1999). Whereas, electrons diffracted in the laser standing wave field (LSWF) mentioned before typically refer to non-relativistic electrons. In contrast, considering a situation where subrelativistic or relativistic electrons launched into a LSWF with characteristics different from those of the weak field cases, the classical theoretical approach often provided the interpretation for the process (Efremov and Fedorov, 1999; Kozák *et al.*, 2018), with the prominence of spatial dependence of the transverse periodic ponderomotive potential $U_p = e^2|\mathbf{E_0}|^2/(m_0\omega^2)cos^2(k\cdot\boldsymbol{r})$, where e is the electron charge, m_0 is the electron mass, $\boldsymbol{r}$ is the position vector, and E_0 is the field amplitude of each wave. Based on the enlightenment of above researches, an electron density modulation reported herein relies on the

© Cambridge University Press 2019

CAMBRIDGE UNIVERSITY PRESS

strong interaction within an ultrashort time between LSWF and electrons. This new scheme of transverse modulation of particle beam has potential for transmission control such as all-optical sub-wavelength local focusing instead of traditional focusing methods.

In this study, we used the particle-in-cell (PIC) simulations for investigation a relativistic electron beam density modulator based on a high-intensity LSWF, and analyzed the impacts of laser intensity or waists on the modulation. We also found that electrons with relativistic velocity launched into an LSWF suffer the reversal of ponderomotive force, which is demonstrated through the particles' velocity distribution and trajectories.

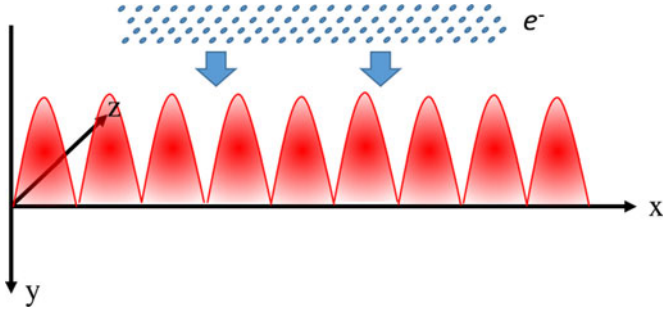


Fig. 1. Schematic geometry of an electron beam launched into a linear polarized LSWF.

The model and simulation results

Two-dimensional (2D) PIC simulations were performed using the EPOCH code (Ridgers *et al.*, 2014; Arber *et al.*, 2015). Figure 1 shows the configuration of the electron beam being launched into the linear polarized LSWF. We assume that the LSWF is generated by two Gaussian linearly polarized laser pulses with the same parameters focused in the y–z plane. They counter-propagate along the x axis launched from the left and right boundaries, respectively, and everything is assumed to be constant in the z-direction for the 2D simulations. The vector potential of the counter-propagating lasers is expressed as $\boldsymbol{a} = a\cos(kx + \omega t)\hat{\mathbf{e}}_y + a\cos(kx - \omega t)\hat{\mathbf{e}}_y$, where $a = a_0 \exp[-(y^2 + z^2)/w_0^2]$, w_0 is the laser beam waist radius, a_0 is the vector potential peak amplitude of one laser normalized by $m\omega c/e$, m and e are the electron's mass and charge, respectively, ω is the frequency of laser, and c is the speed of light in vacuum. The laser wavelength is 800 nm and the duration of the LSWF is 100 fs to allow electrons pass through. Then the electric field and magnetic field of the LSWF are expressed as follows:

$$\begin{aligned}\mathbf{E}(\boldsymbol{x},\boldsymbol{y},\boldsymbol{t}) &= -\partial_t \mathbf{a} = 2a\sin(\omega t)\cos(kx)\hat{\mathbf{e}}_y \\ \mathbf{B}(\boldsymbol{x},\boldsymbol{y},\boldsymbol{t}) &= \nabla \times \mathbf{a} = -2a\cos(\omega t)\sin(kx)\hat{\mathbf{e}}_z.\end{aligned} \tag{1}$$

Considering a relativistic electron beam traveling through an LSWF, the electrons with a Gaussian (an uniform) density profile of 6-μm (1-μm) full width in the x (y) direction are launched along the $+y$ axis toward the overlapping lasers, which is parallel to the electric field of the laser field. The motion of the electrons is governed by the Lorentz force equation, $d\mathbf{P}/dt = -e(\mathbf{E} + \mathbf{v} \times \mathbf{B})$. The peak density of the electron beam is set to be $10^{-3} n_c$ ($n_c = \epsilon_0 m_e \omega^2/e^2$ the critical density for laser with wavelength of 800 nm), which is far below the critical density to avoid the effect of strong space-charge forces on the LSWF. Since the transverse momentum spread of the electron beam caused by the momentum gain after interaction is about 10% of the initial momentum in our case, the initial energy spread of the electron beam, which is well below 10% from a wakefield accelerator or a linac, has little effect on the density modulation. For simplicity, we represent a planar geometry, i.e., the projection of the momentum of the electron onto the direction of the z axis as equal to zero both before and after scattering.

When two counter-propagating traveling lasers form a standing wave, the spatial phase along the propagation direction remains unchanged. Thus, electrons with velocity normal to the direction of laser propagation experience a constant laser phase during the interaction. As Figure 2a shows, the initial electrons of continuous density are modulated into a periodic structure after traversing the LSWF, and the period equals to half the wavelength of the LSWF. Remarkably, each density peak locates at the antinode while each density valley locates at the node of the LSWF. Such discrete electron beam structure is manifested by the special configuration of the LSWF. The electric field value of the LSWF at the nodes remains zero, but the oscillation phases of the amplitude on the two sides of each node are opposite and the electromagnetic field is spatially inhomogeneous. Meanwhile, the electrons traversing across are subjected to the high gradient (i.e., classical ponderomotive force) close to the nodes. The classical ponderomotive force is of the intensity gradient form:

$$\mathbf{F}_\mathrm{p} = -\frac{e^2}{2\varepsilon_0 mc\omega^2}\nabla|\mathbf{E}(x)|^2. \tag{2}$$

It always propels particles toward areas of low field intensity, thus leading to the scattering of electrons owing to the spatial transverse ponderomotive force. We obtain the components of the ponderomotive force as combining Eqs (1) and (2):

$$\mathbf{F}_{\mathrm{p}x} = \Phi \cdot \exp[-2(y^2 + z^2)/w_0^2] \cdot k \cdot \sin(2kx)\hat{\mathbf{e}}_x, \tag{3}$$

where $\Phi = 2e^2 a_0^2/(\varepsilon_0 mc\omega^2) \times \sin^2(\omega t)$. According to Eq. (3), the amplitude maximizes at the phase $kx = n\pi/2 + \pi/4$ ($n = 0, 1, 2, \ldots$) and turns to be zero at the phase $kx = n\pi/2$, i.e., the nodes and antinodes, as shown in Figure 2b, and the ponderomotive force points to the nodes.

Figure 3a shows the distribution of the electron velocity component along the x direction at the corresponding position in the x axis, when the electrons are inside the standing wave field. The entire distribution goes up from left to right and is antisymmetric owing to the Gaussian envelope of the laser pulse which results in the opposite directions of ponderomotive forces in two sides of the zero plane. The result also shows that when electrons enter the LSWF, their velocity distribution in the x direction is periodic. At the antinode planes $kx = n\pi$ ($n = 0, 1, 2, \ldots$), the electron velocity is always zero, the velocities on the left are positive, and those on the right are negative. In other words, the antinodes become the planes of attraction that reverses the typical classical ponderomotive force derived above, thus resulting in the electrons moving toward the position $kx = n\pi$, and further resulting in the gathering of electron beams. The reasons for this reversal of ponderomotive force have been explained (Pokrovsky and Kaplan, 2005). The transverse velocity in the x axis increases with laser intensity for a lager ponderomotive force, but it decreases when the initial gamma increases, for example, $v_x = 5 \times 10^7$ m/s for

https://doi.org/10.1017/S0263034619000338 Published online by Cambridge University Press

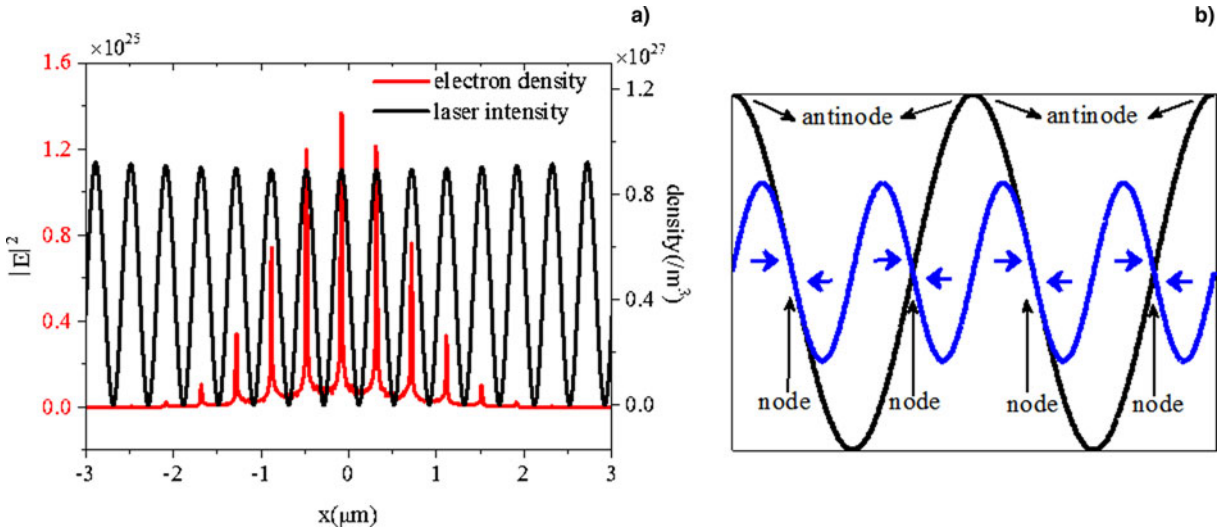


Fig. 2. (a) Electron density integral and laser intensity on the *x*-axis with electron beam energy $\gamma_0 = 20$ and LSWF intensity $I = 1 \times 10^{19}$ W/cm^2. (b) Schematic diagram of phase relation of electric field of LSWF (black line) and the ponderomotive force (blue line), the amplitude is adjusted for a better view.

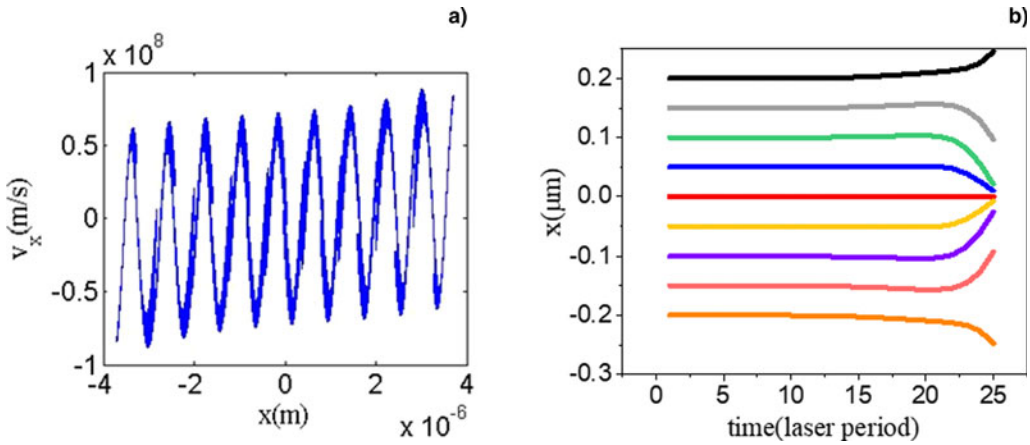


Fig. 3. (a) Distribution of electron velocity component in laser propagation direction (*x* axis) inside the standing wave field at the time of $24\lambda_0/c$. (b) Electron trajectories in the *x* axis for $\gamma_0 = 2$ during the interaction with a linearly polarized laser SW for $a_0 = 0.68$.

$\gamma = 2$ while $v_x = 1 \times 10^6$ m/s for $\gamma = 100$ at the same laser intensity, simply because lower-energy electrons accumulate more transverse momentum when experience longer time in the LSWF. When an electron is launched into the antinode, it suffers the maximal electric field while the magnetic field vanishes. On the contrary, the magnetic field is maximized while the electric field vanishes in the node. The electron launched into this plane suffers an additional Lorentz force induced by the magnetic field $e(\mathbf{v} \times \mathbf{B})$. This Lorentz force associated with the magnetic field depends on the angle between the magnetic field and the velocity of the electron, namely, the oscillation of electrons along the *x* axis is dependent on the polarization direction of the laser. Smorenburg *et al.* (2011) provided the motion equation of electrons in the *x* axis:

$$\frac{d^2k\bar{x}}{d(\omega t)^2} - a_0^2 \frac{1 - 2\beta_0^2 \cos^2\phi}{4(\gamma_0)^2} \sin(2k\bar{x}) \approx 0, \qquad (4)$$

in which electrons entered the LSWF parallel to the *y* axis with initial velocity β_0, ϕ is the angle between the polarization direction and the initial velocity of electrons. In our case, the laser is a linear polarization and parallel to the initial velocity, that is, $\cos\phi = 1$. Thus this equation describes the pendulum-like oscillations in the *x* axis with equilibrium points at $k\bar{x} = n\pi/2$, namely, the nodes and antinodes. Further, the small-oscillation frequency is $\Omega_x(t) = a_0\omega\sqrt{|1 - 2\beta_0^2|}/(\sqrt{2}\gamma_0)$. It is noteworthy that an important critical value is $\beta_0 = 1/\sqrt{2}$ (or $\gamma_0 = \sqrt{2}$), at which the oscillations vanish. When $\beta_0 > 1/\sqrt{2}$, the node planes of $kx = (1/2 + n)\pi$ become unstable; in contrast, the antinode planes of $kx = n\pi$ become stable to attract electrons, as shown in Figure 3a.

The trajectories of the electrons with initial position at node ($x_0 = \pm 0.2$ μm), antinode ($x_0 = 0$ μm), near the node ($x_0 = \pm 0.15$ μm), near the antinode ($x_0 = \pm 0.05$ μm), and the medium ($x_0 = \pm 0.1$ μm) are shown in Figure 3b for the case with $\gamma_0 = 2$ and $a_0 = 0.68$. While traveling through the LSWF, the electrons with initial position at antinode (red line) remain the same position in the *x* axis during the whole process, because the ponderomotive force is always zero in the antinode plane. Electrons between antinode and node move toward the antinode,

https://doi.org/10.1017/S0263034619000338 Published online by Cambridge University Press

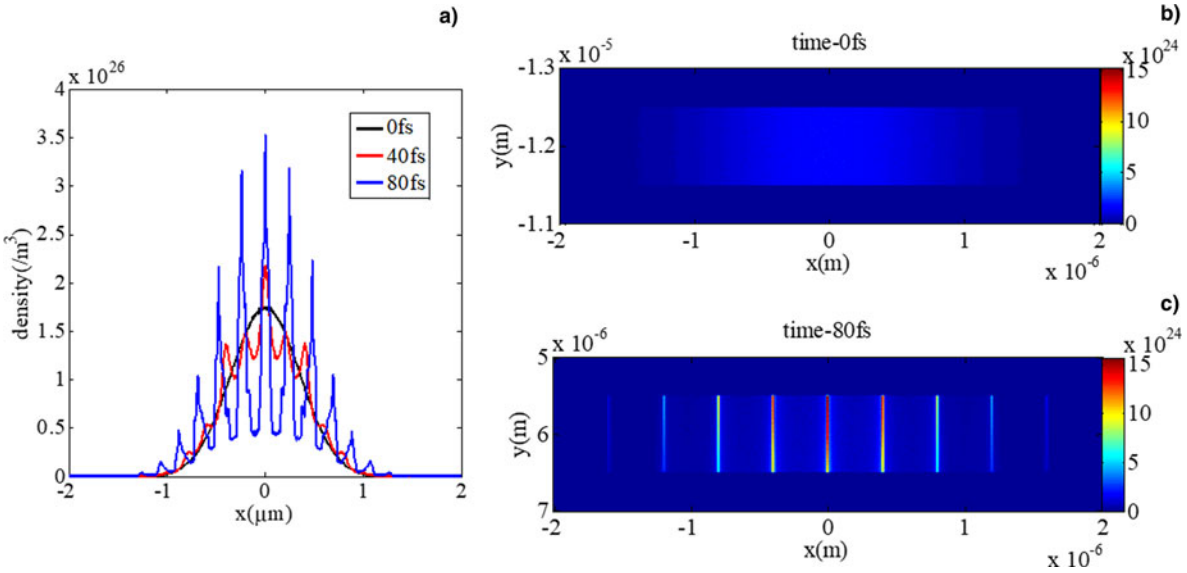


Fig. 4. Evolution of electron density at $\gamma_0 = 2$, $a_0 = 0.68$. (a) The *y*-direction integral curve of electron density distributed in the *x* axis at different evolution times. (b), (c) The electron-density distribution in simulation box at initial moment and 80 fs, respectively.

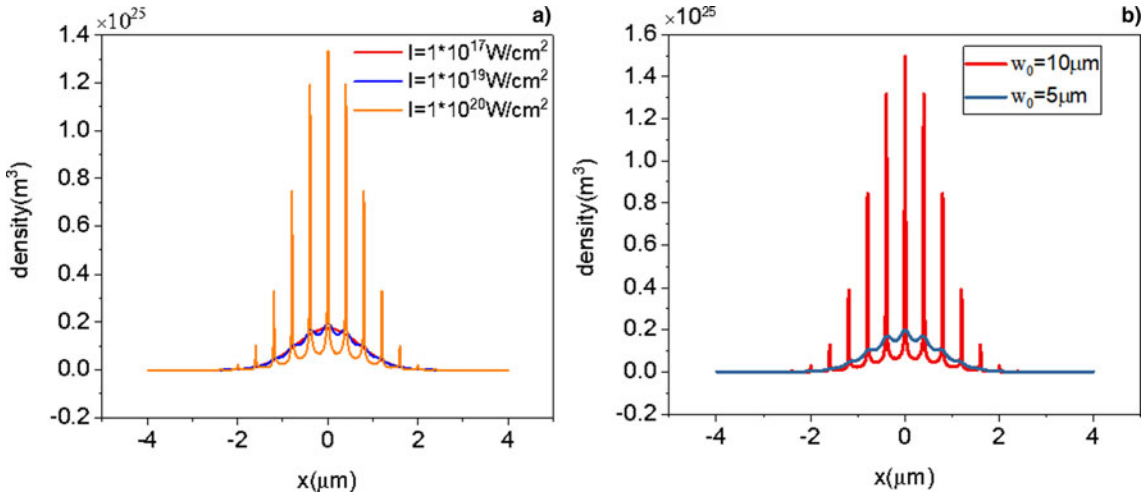


Fig. 5. Electron density along the laser propagating axis after the interaction (a) with different laser intensities for the same $\gamma_0 = 100$, $w_0 = 5$ μm and (b) with different w_0 for the same $\gamma_0 = 100$, $I = 1 \times 10^{19}$ W/cm^2 ($a_0 = 2.16$).

while electrons at nodes move inversely to low field regions deviated from the central antinode due to the opposite directions of ponderomotive forces, which are shown in black and orange lines. These results validate the electron convergence at the antinodes planes as described above.

The interaction between electrons and the LSWF is interesting, and it is a potential technology to access electron density modulator. Therefore, the parameters for this electron beam with laser standing waves are worthy of exploration. Figure 4 shows the evolution of the electron density at $\gamma_0 = 2$, $a_0 = 0.68$. No transverse divergence occurs and the density along the *x* axis with the initial Gaussian distribution transforms into discrete electron peaks at 40 and 80 fs gradually, as shown in the red and blue lines, respectively. The latter has a higher density in each peak, while the whole structure remains Gaussian. Figure 5a shows the electron density after the interaction for the same high energy of $\gamma_0 = 100$ with different laser intensities. At a relatively weak laser intensity of 10^{17} W/cm^2, the final electron distribution through the LSWF is almost unchanged as the same as beginning. By increasing the laser intensity to 10^{19} W/cm^2 ($a_0 = 2.16$), a fraction of the electrons begins to move to specific phases. Further increasing the laser intensity to 10^{20} W/cm^2, sharp density peaks emerged. These results illustrate that the higher the intensity of the LSWF, the more efficient the effect of electron modulation would be. A threshold intensity exists for the initial energy; however, when using a higher intensity exceeding the threshold value, one could use a shorter beam waist, which will be discussed in the following.

The interaction length affects the modulation. The effective modulation length of the LSWF varies with the intensity of the laser. At the same electron initial energy and laser intensity but different beam waists, the electron density after the interaction

https://doi.org/10.1017/S0263034619000338 Published online by Cambridge University Press

differs, for example, different laser beam waist diameters of 5 and 10 μm for the same $\gamma_0 = 100$, $I = 1 \times 10^{19}$ W/cm^2. As Figure 5b shows, the electrons are incompletely separated after the LSWF with a 5-μm beam diameter, accompanied by a high electron density pedestal. However, when doubling the beam diameter to 10 μm, the peak density increases almost 10 times and the density pedestal vanishes but divides into sharp peaks. The whole density remains Gaussian as the initial setting without spatial divergence, causing the electron transverse motion to be limited in the distance of the electron beam length in the x direction. According to Eq. (4), the x motion of electron is simply derived as

$$\begin{aligned} x &= \frac{2ke^2a_0^2}{\varepsilon_0 m^2 c\omega^2} \times \exp\left[-\frac{2(y^2+z^2)}{w_0^2}\right] \times sin(2kx) \times \int [tsin^2(\omega t)]dt \\ &= \frac{2ke^2a_0^2}{\varepsilon_0 m^2 c\omega^2} \times \exp\left[-\frac{2(y^2+z^2)}{w_0^2}\right] \times sin(2kx) \\ &\times \left[\frac{t^2}{4} - \frac{tsin(2\omega t)}{4\omega} - \frac{\cos(2\omega t)}{8\omega^2}\right]. \end{aligned} \tag{5}$$

The interaction time could be simply estimated as $t = w_0/v_0$, where v_0 is the initial velocity of electron in the y direction. Therefore, the laser intensity and the beam waist affect the splitting effect together according to Eq. (5). Considering the two factors discussed above, a good electron beam modulator needs to have a long interaction length or sufficiently high field intensity.

Conclusions

In summary, we used PIC simulations to investigate the interaction of electrons with a high-intensity LSWF. Discrete electron peak structures were observed corresponding to the specific phase of the standing waves of $kx = n\pi$ ($n = 0, 1, 2, \ldots$). The classical ponderomotive force expression was used to describe the motion of electrons in the spatial inhomogeneous standing wave field. However, for our relativistic electrons in a relativistic field intensity, the Lorenz force induced by a magnetic field was also relevant and the direction reverse of the ponderomotive force was observed in the electron velocity and electron trajectory on the axis of the laser for the case $\gamma > \sqrt{2}$. The parameter analysis of the intensity and waist of the laser with electron velocity was performed to demonstrate the condition for an effective modulation. The generation of spatial electron train was a direct and natural consequence of this optical phase-modulation. Our results revealed the potential control for the precision structuring of electron transverse density, with possible applications ranging from ultrafast electron microscopy to accelerator science and free electron lasers.

Acknowledgments. This work was sponsored by the National Natural Science Foundation of China (Grant Nos. 11874372, 11425418, and 61521093), Shanghai Rising-Star Program, Strategic Priority Research Program (B) (Grant No. XDB16), Shanghai Sailing Program (Grant No. 17YF1421100), and Science and Technology on Plasma Physics Laboratory.

References

Arber T, Bennett K, Brady C, Lawrence-Douglas A, Ramsay M, Sircombe N, Gillies P, Evans R, Schmitz H and Bell A (2015) Contemporary particle-in-cell approach to laser-plasma modelling. *Plasma Physics and Controlled Fusion* **57**, 113001.

Bartell L (1967) Reflection of electrons by standing light waves: a simple theoretical treatment. *Journal of Applied Physics* **38**, 1561–1566.

Batelaan H (2007) Colloquium: illuminating the Kapitza–Dirac effect with electron matter optics. *Reviews of Modern Physics* **79**, 929.

Bloch I, Dalibard J and Zwerger W (2008) Many-body physics with ultracold gases. *Reviews of Modern Physics* **80**, 885.

Bucksbaum P, Bashkansky M and McIlrath T (1987) Scattering of electrons by intense coherent light. *Physical Review Letters* **58**, 349.

Bucksbaum PH, Schumacher D and Bashkansky M (1988) High-intensity Kapitza–Dirac effect. *Physical Review Letters* **61**, 1182.

Calendron A-L, Meier J, Hemmer M, Zapata LE, Reichert F, Cankaya H, Schimpf DN, Hua Y, Chang G and Kalaydzhyan A (2018) Laser system design for table-top X-ray light source. *High Power Laser Science and Engineering* **6**, E12.

Chan Y and Tsui W (1979) Classical theory of scattering of an electron beam by a laser standing wave. *Physical Review A* **20**, 294.

Efremov M and Fedorov M (1999) Classical and quantum versions of the Kapitza–Dirac effect. *Journal of Experimental and Theoretical Physics* **89**, 460–467.

Faure J, Glinec Y, Pukhov A, Kiselev S, Gordienko S, Lefebvre E, Rousseau JP, Burgy F and Malka V (2004) A laser–plasma accelerator producing monoenergetic electron beams. *Nature* **431**, 541.

Fedorov M (1967) The Kapitza–Dirac effect in a strong radiation field. *Soviet Journal of Experimental and Theoretical Physics* **25**, 952.

Fiordilino E and Mittleman M (1985) Kinematics of multiphoton ionisation in a laser pulse. *Journal of Physics B: Atomic and Molecular Physics* **18**, 4425.

Flannigan DJ and Zewail AH (2012) 4D electron microscopy: principles and applications. *Accounts of Chemical Research* **45**, 1828–1839.

Freeman R, Freeman RR, McIlrath TJ, Bucksbaum PH and Bashkansky M (1986) Pondermotive effects on angular distributions of photoelectrons. *Physical Review Letters* **57**, 3156.

Freimund DL, Aflatooni K and Batelaan H (2001) Observation of the Kapitza–Dirac effect. *Nature* **413**, 142.

Geddes CGR, Toth C, van Tilborg J, Esarey E, Schroeder CB, Bruhwiler D, Nieter C, Cary J and Leemans WP (2004) High-quality electron beams from a laser wakefield accelerator using plasma-channel guiding. *Nature* **431**, 538.

Germann M, Latychevskaia T, Escher C and Fink H-W (2010) Nondestructive Imaging of Individual Biomolecules. *Physical Review Letters* **104**, 095501.

Gould PL, Ruff GA and Pritchard DE (1986) Diffraction of atoms by light: the near-resonant Kapitza–Dirac effect. *Physical Review Letters* **56**, 827.

Hollis M (1978) Multiphoton ionization and EM field gradient forces. *Optics Communications* **25**, 395–398.

Juffmann T, Milic A, Müllneritsch M, Asenbaum P, Tsukernik A, Tüxen J, Mayor M, Cheshnovsky O and Arndt M (2012) Real-time single-molecule imaging of quantum interference. *Nature Nanotechnology* **7**, 297.

Kapitza P and Dirac P (1933) The reflection of electrons from standing light waves. Conference The reflection of electrons from standing light waves. Cambridge University Press, pp. 297–300.

Kozák M, Eckstein T, Schönenberger N and Hommelhoff P (2018) Inelastic ponderomotive scattering of electrons at a high-intensity optical travelling wave in vacuum. *Nature Physics* **14**, 121–125.

Li X, Zhang J, Xu Z, Fu P, Guo D-S and Freeman R (2004) Theory of the Kapitza–Dirac diffraction effect. *Physical Review Letters* **92**, 233603.

Mangles SPD, Murphy CD, Najmudin Z, Thomas AGR, Collier JL, Dangor AE, Divall EJ, Foster PS, Gallacher JG, Hooker CJ, Jaroszynski DA, Langley AJ, Mori WB, Norreys PA, Tsung FS, Viskup R, Walton BR and Krushelnick K (2004) Monoenergetic beams of relativistic electrons from intense laser–plasma interactions. *Nature* **431**, 535.

Moore C, Moore CI, Knauer JP and Meyerhofer DD (1995) Observation of the transition from Thomson to Compton scattering in multiphoton interactions with low-energy electrons. *Physical Review Letters* **74**, 2439.

Pokrovsky AL and Kaplan AE (2005) Relativistic reversal of the ponderomotive force in a standing laser wave. *Physical Review A* **72**, 043401.

Ridgers CP, Kirk JG, Duclous R, Blackburn T, Brady C, Bennett K, Arber T and Bell A (2014) Modelling gamma-ray photon emission and pair

https://doi.org/10.1017/S0263034619000338 Published online by Cambridge University Press

production in high-intensity laser–matter interactions. *Journal of Computational Physics* **260**, 273–285.

Schaeffer D, Hofer L, Knall E, Heuer P, Constantin C and Niemann C (2018) A platform for high-repetition-rate laser experiments on the large plasma device. *High Power Laser Science and Engineering* **6**, E17.

Sciaini G and Miller RD (2011) Femtosecond electron diffraction: heralding the era of atomically resolved dynamics. *Reports on Progress in Physics* **74**, 096101.

Smorenburg PW, Kanters JHM, Lassise A, Brussaard GJH, Kamp LPJ and Luiten OJ (2011) Polarization-dependent ponderomotive gradient force in a standing wave. *Physical Review A* **83**, 063810.

Tajima T and Dawson JM (1979) Laser electron accelerator. *Physical Review Letters* **43**, 267.

Zewail AH (2006) 4D ultrafast electron diffraction, crystallography, and microscopy. *Annual Review of Physical Chemistry* **57**, 65–103.

Zewail AH (2010) Four-dimensional electron microscopy. *Science* **328**, 187–193.

https://doi.org/10.1017/S0263034619000338 Published online by Cambridge University Press